PHASE SPACE TOMOGRAPHY OF BEAMS WITH EXTREME SPACE CHARGE *

D. Stratakis[#], R. A. Kishek, I. Haber, M. Walter, R. B. Fiorito, S. Bernal , J.C.T. Thangaraj, K. Tian, C. Papadopoulos, M. Reiser, P. G. O'Shea
Institute for Research in Electronics and Applied Physics, University of Maryland, College Park, MD 20742

Abstract

A common challenge for accelerator systems is to maintain beam quality and brightness over the usually long distance from the source to the target. In order to do so, knowledge of the beam distribution in both configuration and velocity space along the beam line is needed. However, measurement of the velocity distribution can be difficult, especially for beams with strong space charge. Here we present a simple and portable tomographic method to map the beam phase space, which can be used in the majority of accelerators. The tomographic reconstruction process has first been compared with results from simulations using the particle-in-cell code WARP. Results show excellent agreement even for beams with extreme space charge and exotic distributions. Our diagnostic has also been successfully demonstrated experimentally on the University of Maryland Electron Ring, a compact ring designed to study the transverse dynamics of beams in both emittance and space charge dominated regimes. Special emphasis is given to intense beams where our phase space tomography diagnostic is used to shed light on the consequences of the space charge forces on the transport of these beams.

INTRODUCTION

For many applications such as free electron lasers, microwave tubes, high-energy injector linacs, a low emittance high current beam is an essential requirement. Such conditions are often difficult to achieve simultaneously. Additionally, these beams are born at low energy and therefore experience strong space charge forces as they are transported from the injector to the induction linac. Space charge forces, if not properly controlled, can lead to deleterious effects such as emittance growth, instabilities, and halo formation [1].

In order to analyze and understand the detailed behavior of the beam transport knowledge of the phase distribution is needed. This is particular important close to the source where space charge forces are still strong. Tomographic methods have been shown in past to recover high quality phase spaces without making a priori assumption of the initial conditions [2]. Tomography is a technique based on the Radon Transform in which a 3D object is reconstructed by assembling information in a series of 2D projections taken from different angles. In the area of beams, one can get projections of the phase space using it's projections in configuration space by either using multi-slit scanners, doing turns on circular machines or using quadrupoles. A summary of previous works [3] is listed in Table 1. Quadrupole scan techniques are most commonly used since they allow the collection of multiple projections without intercepting the beam distribution. The main idea is that a simple variation of the magnet strength rotates the phase space distribution. By appropriate scaling, projections in configuration space are related to projections in phase space. Both scaling factor and angle of the projection are calculated from the beam transport matrix and detailed equations are reported elsewhere [2]. Examples of how projections in phase space are collected are demonstrated in Figure 1. Table 2 contains a summary of previous works in quadrupole-scan tomography. Articles are shorted from top to bottom to according to the generalized perveance defined by

$$K = \frac{qI}{2\pi\varepsilon_0 m(c\beta\gamma)^3} \, , \qquad (1)$$

which is a well known [1] measure of the space charge content of the beam. It is evident, that most works (there is only one exception to our knowledge-last column on Table 1) focus on regimes where perveance is low and therefore space charge effects where neglected. A question arises if tomography is applicable for beams with space charge and if yes how accurate it is.

Table 1: Previous work in transverse phase space tomography

Article	Facility	Method
Fraser et al. 1979	LAMPF	Quadrupoles
McKee et al. 1995	Duke	Quadrupoles
Yakimenko et al. 2003	ATF	Quadrupoles
Li PhD Dis. 2004	UMER	Quadrupoles
Oghaki et al. 2004	KU-FEL	Quadrupoles
Zhou et al. 2006	ATF	Quadrupoles
Hancock et al. 1999	CERN PSB	Mult-turn
Connolly et al. 2002	RHIC	Mult-turn
Anderson et al. 2002	LLNL	Multi-slit
Friedman et al. 2003	HCX	Multi-slit
Minerbo et al. 1981	LAMPF	Three Screen Method

In this paper we will show how tomography can be extended to beams with strong space charge forces. We first, describe the experimental configuration, then simulate the tomography process and test its accuracy and finally report experimental results at University of Maryland Electron Ring (UMER) [4].

Table 2: Studies where quad-scan tomography was applied

Article	Facility	Energy/ Current	Generalized Perveance
McKee et al. 1995	Duke	44MeV / 0.2A	$3.5 \ 10^{-11}$
Oghaki et al. 2004	KU-FEL	10MeV/ 0.1 A	$1.3 \ 10^{-9}$
Yakimenko et al. 2003	ATF	50 MeV/ 100 A	$1.2 \ 10^{-8}$
Zhou et al. 2006	ATF	50 MeV/ 100 A	$1.8 \ 10^{-8}$
Fraser et al. 1979	LAMPF	0.75-100MeV/ 0.018 A	10^{-8}-10^{-5}
Li PhD Dis. 2004	UMER	10keV/ 0.007A	$1.0 \ 10^{-4}$
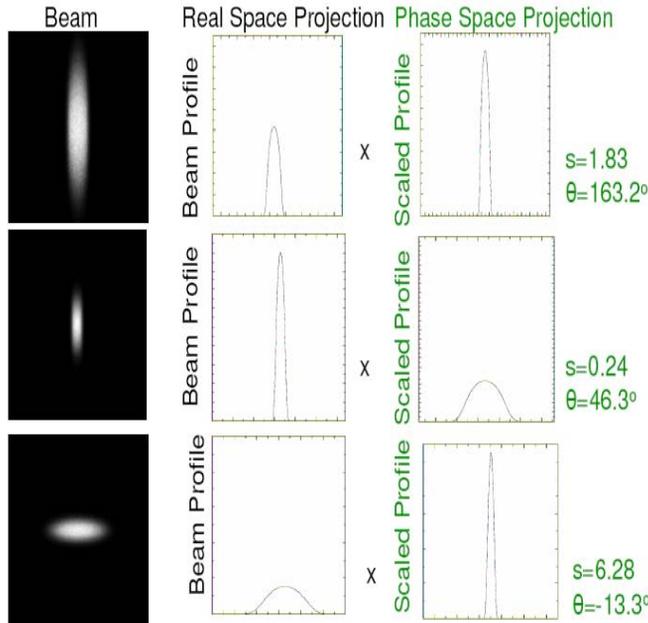
Figure 1: Left side shows the real spatial (x,y) beam photos, the middle shows the integrated x profiles, and the right one shows the scaled profiles.

EXPERIMENTAL CONFIGURATION

Four quadrupoles were employed to rotate the phase space distribution instead of three used previously [5,6]. Such a configuration is more desirable since it allows

reconstruction for more intense beams. Figure 2(a) represents a simplified diagram showing the orientation of this quadrupoles, Fig. 2(b) shows the actual photo. Quadrupoles Q1, Q2, Q3, and Q4 where scanned and a phosphor screen downstream of Q4 displays the electron beam distribution (time integrated over many pulses) and the beam intensity pictures are captured with a 12 bit programmable (CCD) camera (IMPERX-1M48). The beam distributions are projected into x and y axes in order to tomographically reconstruct the xx' and yy' phase spaces, respectively. Each projection is associated with a projection angle obtained from the transport matrix. Details of this process are described elsewhere [6].
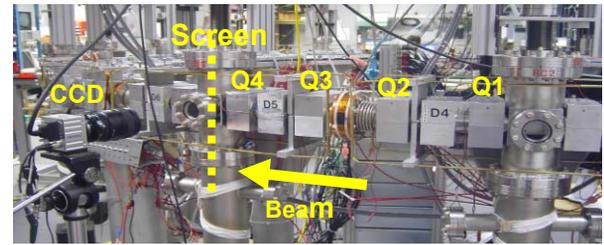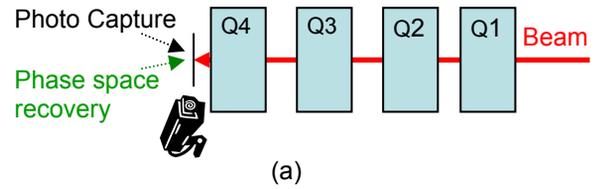
Figure 2: Experimental configuration for phase space tomography on UMER; (a) schematic layout; (b) actual photo

In the presence of space charge, calculation of transport matrix elements becomes more complicated. In order to simplify the analysis some assumptions need to be made about the density distribution and the resulting space charge forces. One method that has been proposed [5] is to use linear space charge forces, which are estimated from the beam envelopes, to correct the transfer matrices between different locations. The detailed process is as follows: Assuming linear space charge forces, the net focusing strengths become [1]

$$\kappa_x = \kappa_{x0} - \frac{2K}{X(X+Y)} \quad , \qquad (2)$$

$$\kappa_y = \kappa_{y0} - \frac{2K}{Y(X+Y)} \quad , \qquad (3)$$

where κ_{x0} κ_{y0} are quadrupole focusing strengths and X, Y are the 2xrms beam envelope sizes for x and y directions, respectively. For a beam were space charge forces can be neglected, the perveance K is low and therefore only the term κ_{x0} and κ_{y0} are used in generating the transfer matrices. However, for a more intense beam the defocusing space charge terms -2K/X(X+Y) and -2K/Y(X+Y) must be included in the matrix analysis.

Calculation of the space charge terms is complicated since knowledge of the beam sizes X and Y is needed. One way to overcome this problem is to solve the beam envelopes using the KV envelope equations [1] given by

$$X'' + \kappa_x X - \frac{2K}{X+Y} - \frac{\varepsilon_x^2}{X^3} = 0 \ , \qquad (4)$$

$$Y'' + \kappa_y Y - \frac{2K}{X+Y} - \frac{\varepsilon_y^2}{Y^3} = 0, \qquad (5)$$

using estimated initial beam sizes and slopes before the first quadrupole and assuming no emittance growth while the beam passes through Q1, Q2 and Q3. We can check our assumptions by comparing the calculated and measured beam sizes at the phosphor screen location. In case they do not agree well we adjust the initial conditions and repeat our envelope calculations until we get agreement. Once, the evolution of X, Y with respect of z is known we can calculate the net focusing functions given by Eq. (2) and Eq. (3). The new transfer matrix can be modeled by the superposition of many hard edge subelements.

SIMULATION RESULTS OF TOMOGRAPHY

In order to verify the quality of the tomography process we simulated the above experimental set-up with the particle-in-cell code WARP [7], developed at the Lawrence Livermore National Laboratory. The advantage of WARP is that it self-consistently includes space charge effects and has been successfully benchmarked against UMER experimental data [4]. For each quadrupole current setting, we run a WARP simulation, collect a snapshot of the beam density in configuration space at the phosphor screen location, and then process it to look like a phosphor screen image. The quadrupole scan results in a large number of photos, each associated with a different projection, and hence a different phase space rotation angle and scaling factor, as defined from the transfer matrix. For image processing we developed a code based on MATLAB. The MATLAB code processes each photo to obtain profiles along x and y, and then scales them to obtain the Radon transform of the phase space distribution. Operating on a number of projections, the code uses the algorithm described in the previous section to recover the original phase space distribution. The tomographic phase space is compared with that generated directly by WARP (independent of tomography). One advantage of this process is that it allows to test the tomographic technique for beams with space charge or beams starting with non-linear distributions. Furthermore, the sensitivity of the technique is established to non linear space charge forces and image forces since these effects are included in the simulation but excluded by the tomography algorithm.

One beam belonging to the space charge dominated regime is selected for our simulation. Beam parameters are: Energy 10keV, current 7 mA, and generalized perveance 10^{-4}. A way to establish the content of space charge within the beam is by calculating the dimensionless parameter χ [1], known as intensity parameter and defined as the ratio of the space charge force relative to the external focusing force. Intensity parameter ranges from 0 (emittance dominated) to 1 (space charge dominated) and in our case it is 0.70. Figures 3 and Fig. 4 demonstrate the recovered phase spaces by Tomography (left) and directly by WARP (right) for beams with two different initial distributions. More specifically, Fig. 3 corresponds to the case where a beam starts with a semi-Gaussian (S-G) initial distribution, which is commonly used for modeling space-charge-dominated beams. In such a distribution the particle density is uniform across the beam, while the velocity profile is Gaussian with uniform temperature. Figure 4 corresponds to the case where a beam starts with a nonequilibrium distribution. The beam is still uniform in configuration space however is hollow in velocity space. The point of this simulation is to illustrate if tomography indeed is not making any assumption about the initial distribution.

Good agreement is achieved for both initial distributions. To quantify our result we measure emittance from both WARP and Tomography phase spaces. We get values that lie within 5% accuracy.
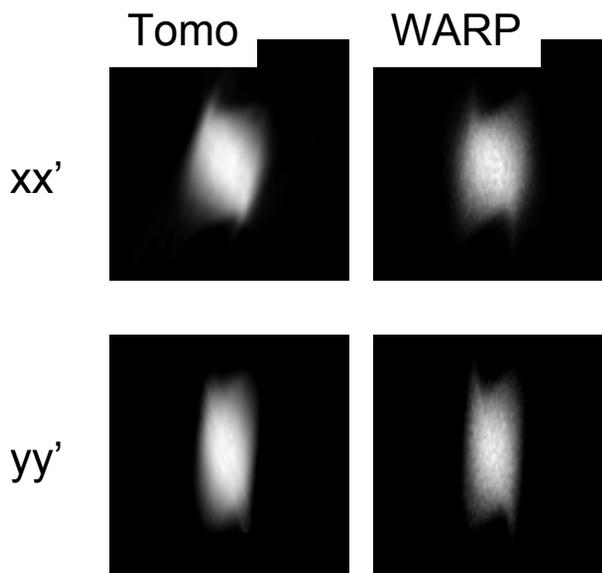
Figure 3: Phase space recovered by Tomography (left) compared to the one obtained directly from simulation (Right). The beam starts initially with a Semi-Gaussian distribution. Note that the phase spaces are shown with subtracted moments <xx'>.

04 Hadron Accelerators

A14 Advanced Concepts

Tomo   WARP

xx'

yy'
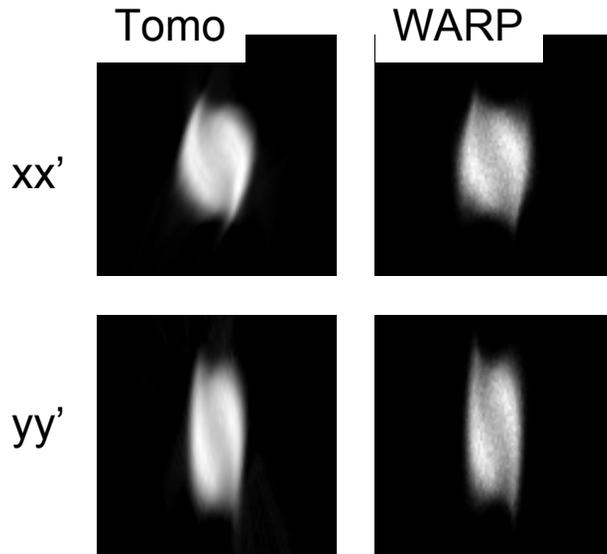
Figure 4: Phase space recovered by Tomography (left) compared to the one obtained directly from simulation (Right). The beam starts initially with a Hollow-Velocity distribution. Note that the phase spaces are shown with subtracted moments $\langle xx' \rangle$.

EXPERIMENTAL RESULTS OF TOMOGRAPHY AND COMPARISONS

Two beams, both belonging to the space charge dominated regime where selected for phase space recovery. Detailed beam parameters are tabulated in Table 3. The experiment is carried at the UMER injector line at the second diagnostic chamber (IC2), placed 76.88 cm from the aperture. In order for the beam to reach IC2, it passes one solenoid (S) and three quadropoles (Q1, Q2, and Q3) after exiting the gun. The locations of S, Q1, Q2, and Q3 are 17.76cm, 40.04, 53.38 and 72.38 cm, respectivey. More details of the electron gun structure can be found elsewhere [8]. The beam current adjastment is made by using an aperture wheel located immediatelly at the exit of the gun. Beam current measurements are performed with a fast Bergoz current transformeter. Quadropole currents were monitored and controlled using Lab-View software. In our experiment the tomography process (quadscan and photo capture) is fully automated. A single measurement take not more than 20 minutes. The layout of our computer control system is illustrated in Fig. 6. Once the MAGNET computer sets the desired magnet values it notifies via text message the TOMO PC to save a beam photo. Then an aknowledgement message is send back to the MAGNET PC. This process continues until the quadrupole scan process is over.

A phase space measurement requires close to 200 projections. The quadrupole strengths are choosen in a comprise to: (1) rotate the phase space distribution close to 180 degrees; (2) keep the beam focused within the screen boundaries; (3) avoid the beam hitting the pipe and reduce effects from image forces.
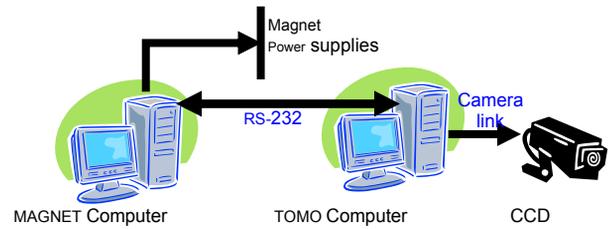
Figure 5: Schematic layout of the computer hardware used for automated phase space tomography.

Table 3: Beam parameters at the experiment. Both beams belong to the space charge dominated regime.

Energy, keV	10	10
Generalized Perveance	$6.7 \, 10^{-5}$	$2.8 \, 10^{-4}$
Current, mA	4.5	19
Beam size at the aperture (mm)	0.875	1.5
Current, mA	4.5	19
Pulse Width, ns	100 ns	100 ns
Intensity parameter, χ	0.62	0.85

Figure 6, top part, demonstrates the distribution in configuration space, as well as the measured distribution in the (x, x') and (y, y') planes in IC2 for the 4.5 mA beam. The distributions correspond to the case where the Peak Magnetic Field strength of the solenoid is 98.1 G and the three quadrupoles have currents -1.32A , 2.2 A, and -2A, respectively. An observed pattern within the beam distribution in real space is believed to be the image of the grid, which is placed within the Anode-Cathode gap. It is well known that in beam physics, in parallel with light optics, a lens (in our case the magnets) can form an image of an object downstream. Additionally, the measured distributions give evidence of halo particles.
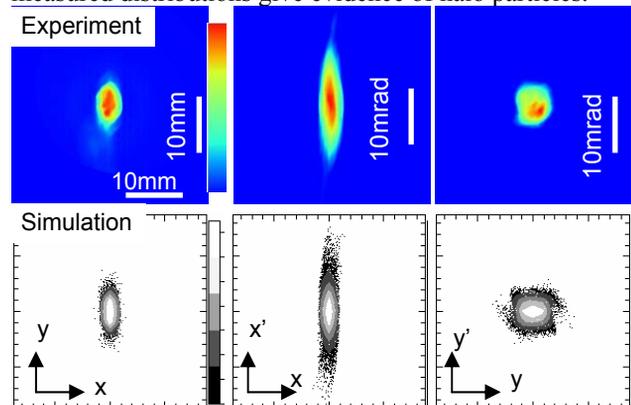
Figure 6: Phase space mapping of the 4.5 mA beam in IC2; using tomography (top row); using WARP simulation (bottom).
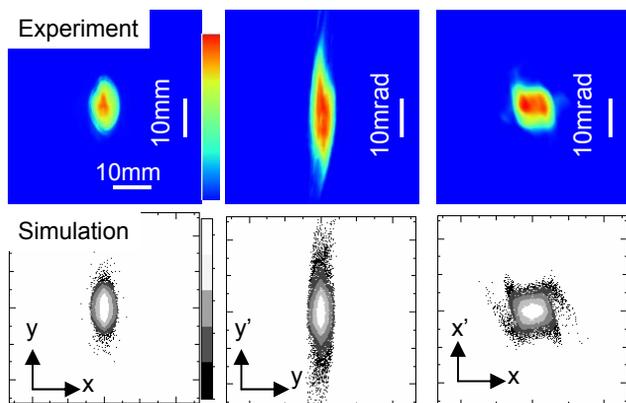
Figure 7: Phase space mapping of the 19.0 mA beam in IC2; using tomography (top row); using WARP simulation (bottom).

Figures 7, top part, show the measured distributions for a more intense beam (current is 19mA). Magnet settings are the same as the 4.5mA beam. Again the measured distributions give evidence of halo particles surrounding the main core, especially, at the (y'y) phase space.

To aid in understanding of the experiment, we have conducted PIC simulations using the code WARP. Knowledge of the exact initial distribution is not known, however, in the simplest approximation the beam emerging the cathode was modeled with a semi-Gaussian distribution, i.e., one that is uniform in space, but has a Gaussian velocity distribution. As it is evident from these figures halo particles are also seen in the simulations, and agreement between experiment and simulation is good, especially for the lower current beam. Future simulations with more complex initial distributions are underway.

Knowledge of the phase space distribution allows us to retrieve information of other important parameters like the beam emittances and the beam slope. Our measured parameters are listed in Table 4. Such information is very important, especially when simulating the experiment since they provide insight of the initial conditions.

Table 4: Important beam parameters collected in IC2 from the reconstructed phase space plots

Parameter	4.5 mA	19.0 mA
ε_x, μm	19.4	44.5
ε_y, μm	15.8	47.7
x_{rms}, mm	0.99	1.65
y_{rms}, mm	1.87	3.16
xp_{rms}, mrad	7.2	7.0
yp_{rms}, mrad	7.1	15.5

In order to get an estimate of the quality of our results we compare the measured emittance values to that expected at the gun aperture. Assuming a uniform configuration space distribution in the aperture plate, we estimate the emittance of the 4.5 mA to be 16.4±5.0 mm·mrad, approximately, by scaling it with the full beam

(the radius and the emittance are 3.2 mm, 60±20 mm·mrad for the full beam; the radius is 0.875 mm for the 4.5 mA beam). Repeating the same process for the 19.0 mA we get 28.2±9.0 mm·mrad. Both tomographic measurement are within the expected limits. However, the slightly higher value measured for the 19.0 mA beam is believed to be related with the halo particles clearly seen in Fig. 7. It is well known that halos are associated with emittance growth [1].

CONCLUSIONS

We have developed a phase space tomography diagnostic for beams with space charge. This is achieved by adding a linear term due the space charge in our algorithm. Simulation of the Tomographic process using particle in cell codes indicates good agreement with our Tomographic reconstruction even for beams with extreme space charge or for beams with non-linear distributions. Finally, experimental data using tomography are been reported. Results show high quality phase space maps and indicate the presence of halo particles. Future experiments within the UMER ring and comparisons with PIC simulations with WARP are underway.

AKNOWLEDGEMENT

REFERENCES

[1] M. Reiser, *Theory and Design of Charge Particle Beams*, (John Wiley & Sons, Inc., New York, 1994)

[2] C. B. McKee, *et. al., "Phase space tomography of relativistic beams,"* Nucl. Instru. Methods Phys. Res. A 358, 264 (1995)

[3] J. S. Fraser, IEEE Trans. Nucl. Sci. NS-26, 1641 (1979); R. Connolly et al. Nucl. Instrum. Methods Phys. Res. A **443**, 215-222 (2000); S. Hancock et al. Phys. Rev. ST Accel. Beams **3**, 124202 (2000); C. Montag et al. Phys. Rev. ST Accel. Beams **5**, 082801 (2002); V. Yakimenko et al. Phys. Rev. ST Accel. Beams **6**, 122801 (2003); S. G. Anderson, *et al.,* Phys. Rev. ST Accel. Beams **5**, 014201 (2002); H. Ohgaki et al. Nucl. Instru. Methods Phys. Res. A 528, 366 (2004); Friedman *et al.* Laser and Particle Beams 21, 17 (2003)

[4] R.A. Kishek, *et. al., Physics of Plasmas* **10**, 2016-2021 (2003).

[5] H. Li, Ph.D. Thesis, University of Maryland, 2004;

[6] D. Stratakis, *et al., Phys. Rev. ST Accel. Beams* **9**, 112801 (2006).

[7] A. Friedman, *Nucl. Instrum. Methods Phys. Res.A* **544,** 160-170 (2005).

[8] T. Godlove, *et. al.*, Proceedings of 1999 PAC, New York, NY, 1999.